

## TRIBOLOGICAL PROPERTIES OF DLC AND GLC COATING FOR AUTOMOTIVE ENGINE COMPONENTS APPLICATION UNDER LUBRICATION

Riyadh A. AL-SAMARAI\*

Electromechanical Engineering Department, Engineering College, University of Samarra  
Samarra, 34010–Iraq, IRAQ  
E-mail: riyadh2824@yahoo.com

Y. AL-DOURI

Department of Mechanical Engineering, Faculty of Engineering, Piri Reis University  
Eflatun Sk. No:8, 34940 Tuzla, Istanbul, TURKEY  
Nanotechnology and Catalysis Research Centre, University of Malaya, 50603 Kuala Lumpur, MALAYSIA  
Department of Applied Physics and Astronomy, College of Sciences, University of Sharjah,  
P.O. Box 27272, Sharjah, UNITED ARAB EMIRATES

Modern automotive designs are needed to increase mechanical and thermal loads that have longer lifespans and are lighter. The power transmissions and motors often use low-friction hard coatings to prevent wear and reduce friction. The Cr-doped graphite-like carbon method is employed for evaluating coating friction and responses to chromium-doped graphite-like carbon (Cr-GLC) under lubrication. Cr-GLC coatings and chromium-doped diamond-like carbon (Cr-DLC) coatings are arranged using physical vapor deposition (PVD) and plasma-enhanced chemical vapor deposition (PECVD), respectively. The results have demonstrated in comparison to the dry friction coefficient, the friction coefficient under lubrication conditions has been reduced by 40%. Due to its excellent frictional physicochemical properties and compact microstructure, Cr-DLC has an optimum tribological resistance that is significantly higher than that of Cr-GLC. Viscosity, corrosivity, and coating microstructure are used to measure the impact of composite elements. The most ideal characteristics of the Cr-GLC coating are attributed to the non-reaction of additives in oil with friction surfaces.

**Key words:** engine components; complex coatings; Cr-GLC; Cr-DLC; lubrication.

### 1. Introduction

Modern engine designs aim to improve fuel efficiency and minimize toxic emissions while maintaining more vehicle power. Technologies such as turbocharging and direct gas injection are used [1, 2]. Amorphous carbon coatings are used in the aerospace industry in microelectronic devices in several fields due to their excellent tribological and mechanical properties [1, 2]. Studies on DLC with ZDDP or other anti-wear and extreme pressure (AW/EP) additives have been done recently, however, the outcomes are mostly inconsistent. Some studies claim that (ZDDPs) create tribofilms on coatings of DLC [11-14], but others deny this or claim that there is no tribochemical reaction between the DLC and the additive [7-10]. In order to identify the differences between the DLCs, it is crucial to comprehend why such disparate outcomes have been discovered [3-6]. Coatings of (GLC) are popular in a number of applications because they are made from  $sp^2$ -bonded carbon, which has a self-lubricating effect. They can serve as a working surface for sea water shear components [7-9]. According to Lee *et al.* [10] potential bearings coated with (DLC, GLC), and

---

\* To whom correspondence should be addressed

CrN with sliding friction under different circumstances, the bearing capacity should be inversely proportional to the bearing roughness, coating depth and mechanical characteristics.

To demonstrate the disadvantages of boundary lubrication, Aboua *et al.* [11, 12] investigated friction using DLC coatings and then found that carbon diffusion is the main factor affecting the properties of hydrogenated amorphous carbon coatings. According to Bouchet *et al.* [13], ZDDP-based tribofilms were produced. Despite contradicting information on comparable forms of DLC, our experiments on highly hydrogenated DLC with 50% at.% H demonstrates that hydrogen concentration has a sizable impact on the film-forming ability of DLC coatings [16]. When adopting the arc plating process, the thick CrN coating has demonstrated outstanding load-bearing capability, long-term wear resistance, increased corrosion resistance, and better thermal stability [5, 6]. Solid lubricants provide effective anti-friction and wear-resistance properties. However, lubricants that are subjected to hovering or heavy loads have a difficult time maintaining their quality over an extended period of time. However, the use of liquid lubricants is limited due to their volatility and heavy reliance on the environment. Traditional solid and liquid lubricants cannot meet the demands of new machinery. Solid-liquid composite lubricating systems can be more effective when the advantages of each component are successfully combined while minimizing their disadvantages [7]. Because of things like the lack of coating, CrN loses its ability to reduce friction in the presence of lubrication or in low/high rotation temperatures [5-8]. Coatings are the most significant and readily available lubricant additives, and they are one of many factors that can reduce friction [9-12]. However, comparing the impact of both coatings (DLC and GLC) on the properties of the composite under structure lubrication is practically impossible [13, 14, 19]. To consciously employ surface and lubricant together to maximize performance, however, is challenging. To understand the functioning of the tribofilm in light of surface tribochemistry and the compatibility of the GLC surface with oil composition, current work has evaluated the potential effect to reduce friction and slow wear due to the presence of Cr-GLC and Cr-DLC coatings. For this purpose, two coating samples of both mentioned coatings were evaluated at various lubrication conditions.

## 2. Experimental procedure

### 2.1. Materials

The coatings of Cr-GLC and Cr-DLC are used for Al-Si alloys. The deposition machine has four target positions with a vacuum commanded by mechanical and molecular pumping. A sample of Al-Si alloys ( $\phi = 15 \text{ mm}$ ) is used to test the tribological properties. Al-Si alloys are used as a substrate to study the chemical composition of two coatings. Before being re-polished and before spraying, all substrates are subjected to ultrasonic centrifugation and alcohol for 15 min. To remove oxides, metal, and silicon wafers are cleaned by bombardment with cleaning. A period of 10 minutes and a voltage of 400 V is used when testing coatings of (Cr-GLC) and (Cr-DLC), respectively.

Table 1. Characteristics of Cr-GLC and Cr-DLC coatings.

Coating		Target Cr (KW)	Target C (KW)	Ar (sccm)	C4H10 (sccm)	Voltage of biase (V)	Technique for depositing
GLC	Cr	0.102	0.04	14	–	350	PVD
	Cr-C	1.24	0.2	14	–	50	
	Cr-GLC	0.101	2.1	14	–	50	
DLC	Cr	0.07	–	24	0	350	PECVD
	Cr-C	1.21	–	24	15	50	
	Cr-DLC	0.11	–	22	25	50	

The Cr layer is usually used as a buffer layer to improve adhesion. Pure graphite is used as a carbon source. Table 1 lists the parameters used. To assess the wettability at the coating surfaces, measure the contact angles at room temperature using a directional contact device (OCA20, Data Physics, Germany). In this research, Cr-GLC and Cr-DLC had wettability values of 7.12 and 8.11, respectively.

## 2.2. Structure of investigated coatings

Scanning electron microscopy (SEM, 7610F, Japan) and its EDS have been used to investigate the morphology of the moving region and coverage. The total roughness, Ra along with the centreline of coatings is used on the silicon wafer at a distance of 1  $\mu\text{m}$ . The bond form of carbon atoms in the coatings is utilized for atomic force microscopy (AFM) (ESCALAB 250Xi, Thermo Scientific XPS, USA), which is used to characterize the states of two coatings. Samples were measured five times to guarantee the accuracy of the results on a microhardness tester with a nanoindenter (MTS ) and an indentation depth of 250 nm. Scratches are commonly used to test the adhesive deformation between substrates and coatings (MFT-4000, China, Instrument Technology, ) at a load of 30 N. Three measurements are made for each pattern.

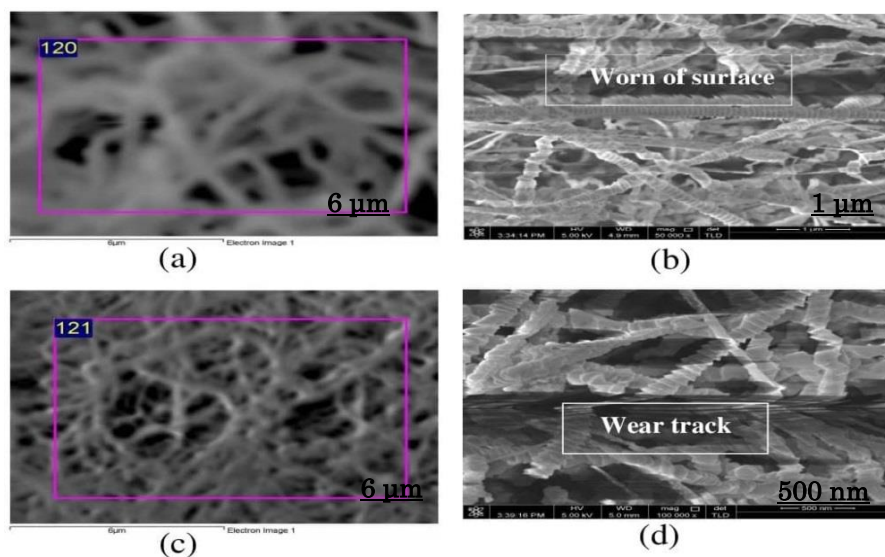


Fig.1. SEM images of (a) coating surface (Cr-GLC); (b) (Cr-GLC) cross-section; (c) coating surface (Cr-DLC); and (d) (Cr-DLC) cross-section.

## 2.3. Friction testing

Pin-on-disc (CSM, Switzerland), tribological tests are carried out in spinning mode under dry and lubricated sliding conditions. The diameter of the pin, previously made of aluminum-silicon alloy after the coating process, is 10 mm. The slip has a length of 1500 m, temperature of 28 °C, 65% relative humidity, speed of 200 rpm (~0.06 m/s), and loads of 10, 20, and 30 N were applied. SEM and AFM are used to analyse the topography and morphology of the worn surfaces by measuring a 3D profile, a minimum value of 67% was achieved with reduced friction. Components can adapt to abnormal friction conditions due to the presence of GLC. Figure 7 also exhibits the average values of friction coefficients for two coating samples at various lubrication conditions. The GLC film performed well, and the upper GLC film greatly reduced wear. On its own, the GLC's self-lubricating nature cannot provide the performance required; In addition, the oil's tribochemical reactions also played a role in this process. The chemical composition is indicated via an EDX analyzer. The adhesion of the coating is used to evaluate scratch (CSM Reve test) with an acoustic emission detector, the radius needle is 0.2 mm with 120 cone perspective,  $W$  is the degree of overlap,  $V$  is the number of overlaps,  $N$  is load and  $S$  is a total distance.

### 3. Results and discussion

#### 3.1. Structure and morphology

Possible interfacial interactions between lubricants and coated surfaces have been identified using SEM-EDS. Figure 1 depicts the shape and permeability sector of the two coatings. Following tribological tests, an SEM is used to look at the shape of the applied tracks. The dense particles are found on the surface of each coating, as seen in Figs 1a and c. The buffer layer of Cr, the Cr-C intermediate layer, and the top layer of Cr-GLC are among the moving parts of the Cr-GLC coating that can be diagnosed using EDS. The buffer layer of Cr is made up entirely of Cr elements. The intermediate layer of Cr-C, which is made up of Cr and C with a Cr content, comes after the buffer layer. The top layer with 6.81% Cr and 93.19% C.(Fig.1b) of (Cr-GLC). EDS is typically used to determine the levels of Cr and C.

The presence of the Cr buffer layer discovered by EDS and the Cr-C columnar layer is confirmed by the dense (Cr-DLC) layer, the Cr-C columnar layer, and the (Cr-DLC) direct coating. Columnar Cr-C layers made of Cr and C are normally formed as the material composition of a Cr-containing fabric declines from inner to outer. The percentage of (Cr-DLC) that is dense is 7.33 and 92.67%, respectively (Fig.1d). To accurately assess how structure affects performance, coating thickness must be determined. The thickness of the Cr-GLC is  $1.93 \mu\text{m}$ , while the Cr-DLC is  $1.94 \mu\text{m}$  thick. a hierarchical structure was visible in the cross-section of the surface to the steel substrate. A deep intermediate layer of (Cr-DLC) measuring around  $35 \mu\text{m}$  thick made up the coating's total thickness of about  $34 \mu\text{m}$ . This layer arrangement, while coating Cr-GLC  $35 \mu\text{m}$  thick, improved the coating's toughness to handle the higher load and wear as well as strengthened the GLC film's adhesion to the steel substrate [28].

#### 3.2. AFM characterization

Good topography and tribological properties [20-22] are crucial. So, the coated surfaces are examined using AFM. In order to evaluate worn (Cr-DLC) and (Cr-GLC) surfaces, AFM-EDS implies that factors O, Fe, P, Zn, S, C, and Ca will be present. Figure 2 depicts the microstructure of the coating and surface roughness. The coatings' robust structure and homogeneous particle dispersion make them durable. In comparison to the Cr-GLC coating, which has a roughness of  $6.667 \text{ nm}$  as opposed to  $0.806 \text{ nm}$ , the Cr-DLC coating is smoother. A friction and wear tester that technically matched the DIN51834 standard for Pin-on-disc contact geometry was used to assess the friction and wear properties of the two coating samples. Each sliding test was performed three times, with different friction coefficients. Before testing, samples were cleaned in acetone for five minutes. Several working circumstances were developed in this study to assess the effectiveness of wear and debris marks (see Tab.2).

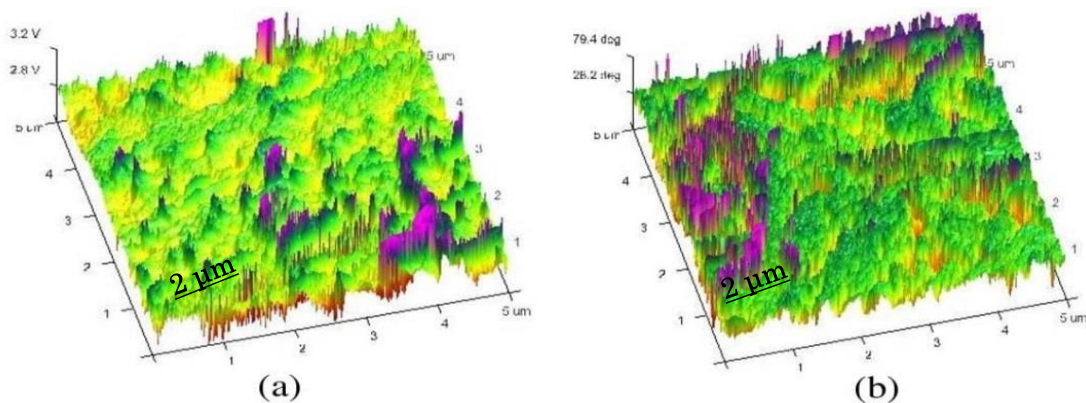


Fig.2. AFM coating images for (a) (Cr-GLC) and (b) (Cr-DLC).

### 3.3. Strength of adhesion investigations

The cohesive pressure between the substrate and the coating will simulate the composition and fracture toughness of the coating. It is known that materials with excessive adhesion stress have better fracture resistance [40-41]. When a normal load is applied, adhesion and frictional stress, or the largest gap between the coating and the substrate, have different effects [42]. The electrical adhesion force of the Cr-DLC coating is  $30\text{ N}$ , while the energy of the Cr-GLC is  $28.3\text{ N}$ , as shown in Fig.3. This finding suggests that the Cr-DLC coating has a stronger resilience to breaking than the Cr-GLC coating. The frictional pressure changes as anticipated under the applied loading, which is consistent with adhesion, which is the separation between the coating and the substrate [42, 43]. Utilizing the phonon emission signal's detecting component, coating adherence was assessed. It has a diamond needle radius of  $0.2\text{ mm}$  and a taper angle of  $120^\circ$ . Scratch tests employed a  $0\text{-}30\text{ N}$  load gauge,  $5\text{ mm/min}$  scratch speed, and  $5\text{ mm}$  scratch distance. Before each scratch test, the coated surface and diamond needle were cleaned with isopropanol. The acoustic emission signal and the coefficient of friction are promptly recorded when coatings degrade under critical loads. While it can alternatively be the value of the coating's bearing capacity, the critical load in this work was defined as the full removal of all coatings from the scratch channel. To determine if the tribofilms show any differences in adhesive properties depending on the hydrogen content of the coatings, AFM was used to create shear force maps and force-displacement curves[42, 44].

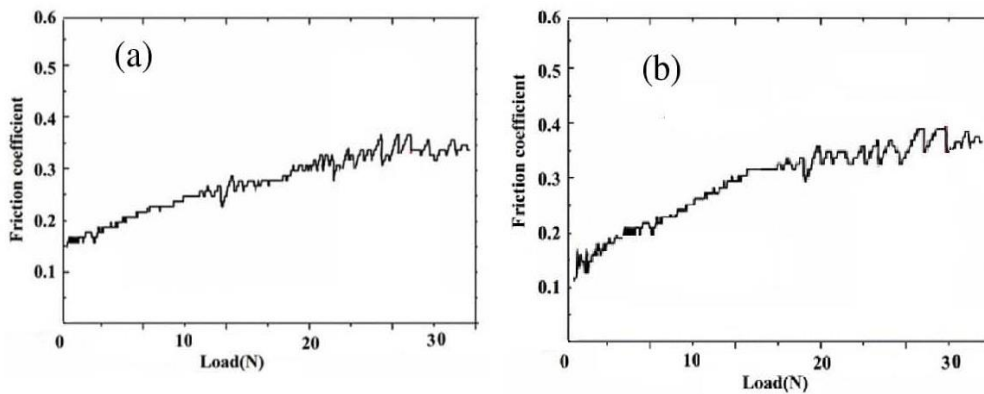


Fig.3. Friction coefficient of coating (a) (Cr-GLC); (b) (Cr-DLC).

### 3.4. Wear rate

Figure 4 shows two coatings under lubricant conditions. (Cr-DLC) is regarded as being superior to (Cr-GLC) due to its higher hardness and higher  $\text{sp}^3\text{C}$  binder content. In order to stop cracks from spreading, the coating of Cr-DLC also offers better anti-wear qualities and higher (H/E) and (H<sup>3</sup>/E<sup>2</sup>) values. The initial wear rate of the Cr-DLC is 26.67% less than that of the Cr-GLC coating. The greatest percentage is 58.72% for Cr-GLC. The statistics gathered demonstrate that liquid lubricants' anti-wear qualities have greatly improved. Additionally, tribochemical reaction films produced by friction might minimize wear [45]. Summarising the data, we can say that the physicochemical circumstances, which are superior in terms of wear resistance, influence enhance the wear resistance of (Cr-DLC) of use. The relationship between the coating friction coefficient curves (Cr-DLC and Cr-GLC) during a scratch test is depicted in Fig.7. The frictional properties of coatings of (Cr-DLC) and (Cr-GLC) with full lubrication are shown in Fig.7. Depending on the lubrication conditions, the coefficients of friction (CTE) for both coatings changed. The (Cr-GLC) contact produces a substantial dry slip friction of roughly 0.7 due to the higher interfacial shear strength [6], but the rubs create a low and consistent friction coefficient of 0.25 (see Fig.7c). The self-lubricating properties of the coating of (Cr-DLC) and the creation of amorphous graphitic carbon that is transmitted to the opposing surface are credited with the superior performance [4, 14].

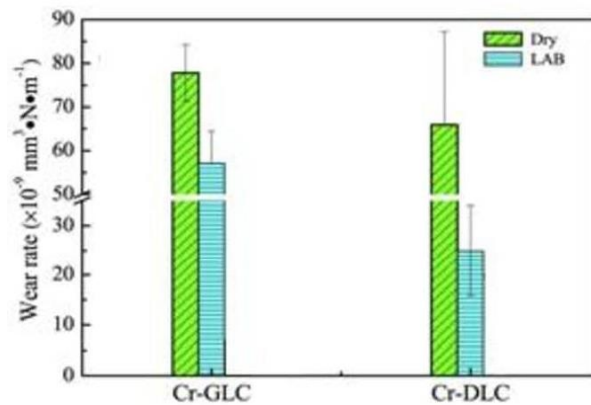


Fig.4. Wear analysis of coating of Cr-DLC and Cr-DLC under dry and lubrication sliding.

### 3.5. Raman analysis

The Raman peaks typical of the coating of the DLC insurance scheme give heights of  $D$  at  $1.350 \text{ cm}^{-1}$  and  $G$  at  $1.580 \text{ cm}^{-1}$  while the coating of (GLC) peaks reach  $D$  at  $1.350 \text{ cm}^{-1}$  and  $G$  at  $1.560 \text{ cm}^{-1}$  [10, 24]. In Fig.5, the approximate Gaussian spectra of the various Raman coatings are shown. The distinguishing peaks of the (Cr-GLC) coating are situated at corresponding separations of  $1372.9$  and  $1554.3 \text{ cm}^{-1}$ . A specific height of  $1372.9$  and  $1554.3 \text{ cm}^{-1}$  is where the coating of (Cr-GLC) peaks are found [15, 16, 25]. But the  $D$  height and  $G$  peak of the Cr-DLC covering are approximately  $1310.8$  and  $1527.2 \text{ cm}^{-1}$  respectively. Within this study, this can also be explained by the fact that the mixed layer of carbon (either in its original or graphitized form) and the tribofilm on these surfaces had stronger cohesive forces than the original surface. However, compared to the combination, the bond strength of most DLC was significantly higher.

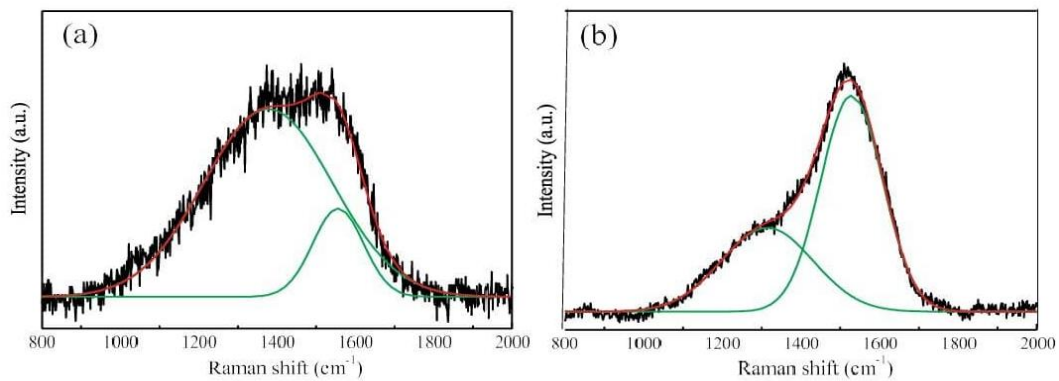


Fig.5. Raman spectra of coating of (a) Cr-GLC; (b) Cr-DLC.

The  $G$  peaks converge towards each other to constrain each layer, in contrast to the common  $G$  peaks as seen from the edge of each layer that is relatively far apart [17, 25]. While the coating with Cr-DLC has a thermal height of  $1527.2 \text{ cm}^{-1}$ , we notice the height of the coating with (Cr-GLC) is usually  $1554.3 \text{ cm}^{-1}$ . Since the coating of DLC contains a lot of  $\text{sp}^2\text{C}$  and  $\text{sp}^3\text{C}$  hybrid bonds, the upper half of the  $G$  is often wider and has fewer waves in the lateral direction than the Cr-GLC coating. We also note that in coatings with low  $G$ -vertex widths, there is a link between the selective resonance emission of  $\text{sp}^2$ -linked  $\text{sp}^2$  carbon clusters of different sizes and  $\text{sp}^3$  carbon ratios [18, 26, 27]. The special ratio can be used to determine the tissue abundance of  $\text{sp}^3$  C-ligands. The results show that the ratio of (Cr-GLC) to (Cr-DLC) was around  $4.81$  for Cr-GLC and  $0.55$  for

(Cr-DLC) [41]. When necessary, metal oxides can be chemically broken down to (FePO<sub>4</sub>) to generate easy shearing qualities. The coating compounds bind different grain sizes to the ultrafine phases of the nanocrystals. It was advantageous to deflect and stop the growth of large fractures when maximum contact pressure occurred because the amount of oxide debris on the nanoscale would maintain a reasonably high hardness at the friction interface. Since carbon has lower shear resistance than other materials, it was added to the coating matrix which reduced wear, friction, and scuffing due to metal sulfides [19, 23-25].

### 3.6. Hardness and elastic modulus investigations

Solid coatings usually have good tribological properties during practical application [32-34]. To reduce the matrix effect, the indentation depth to coating depth ratio is approximately 10% when tested [33-35]. Figure 6 shows the modulus of elasticity (E) and (H) for two different layers. The modulus of elasticity and toughness for the coating of (Cr-GLC) were 12.90 and 146.55 GPa respectively, and 19.50 and 176.44 GPa for the coating of Cr-DLC respectively. Although in solution the hardness of all coatings was relatively comparable both initially and after 2 hours of friction, as can be shown in Fig.4, the first friction is probably caused by the high sp<sup>2</sup> content, but it is not retained during subsequent friction in the base oil. The early DLC border friction in base oil and solution is compared in Fig.4. For all coatings, the effect of wear quickly lowers interfacial friction. This might be because the thin film in DLC blocks the naturally low friction feature of graphite. After two hours, the DLC's final coefficient of friction is still lower than the majority of other coatings. Surprisingly, DLC displays 2 hours of friction resulting in a substantial reduction in friction. This is most likely because friction causes graphite inclusions in the covering to be exposed, which reduces friction [16]. After two hours of friction, DLC exhibits a minor reduction in interfacial and semi-dry friction, but its friction of (Cr-GLC) is higher than that of Cr-DLC coating. This might be a result of coating wear, as seen in Fig.7, which displays a particularly rough surface in comparison to other DLC [36-39].  $\mu$  is equal to  $0.78 r^2 (H^3/E^2)$  [7], where r is the contact radius. Higher values of (H/E) and (H<sup>3</sup>/E<sup>2</sup>) can be found on the coating of Cr-DLC (Fig. 6b), indicating an improvement in plastic deformation resistance and fracture toughness.

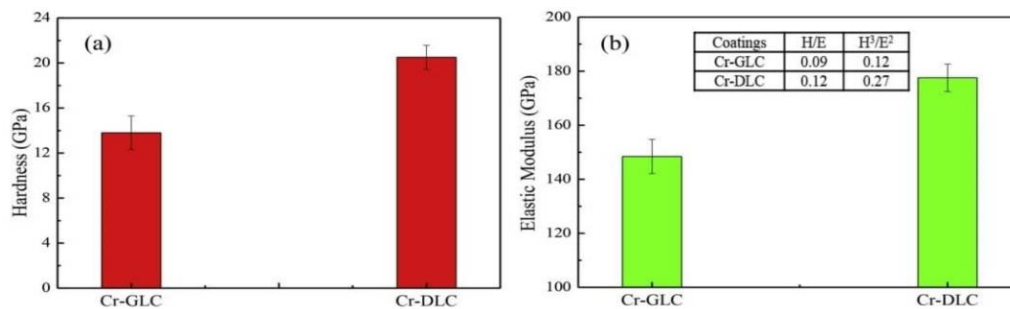


Fig.6. (a) The hardness of coatings; (b) Modulus of elasticity for coatings.

Table 2. EDX for wear and debris marks.

(Point)	( C %)	( O %)	( Fe %)	( Cr %)
A	66.2	9.36	7.32	7.45
B	71.62	1.31	12.56	7.78
C	62.11	3.00	0.36	27.10
D	61.13	3.31	27.11	0.26

### 3.7. Friction and imparting

Figure 7a and b shows the friction coefficient and slip distance for each layer in a dry slip. The two phases that make up the Cr-GLC coating's coefficient of friction on Al-Si alloy are described in more depth

below. The coefficient of friction of Cr-GLC coating initially rises and then steadily falls as the lubricating and sliding film progresses through the phase. The friction of the coating gradually rises and then surprisingly reduces as a consequence of the continuous sliding process under lubrication and a result of the friction grooves created by the abrasive particles in the Cr-GLC coating. The coefficient of friction curve of the Cr-DLC coating appears at a specific amount along the sliding track. One crucial element is the significant quantity of  $sp^3$  C binder, which results in it challenging to create a graphite switching film due to the protracted stabilization step of the friction coefficient. In order to prevent the development of C-C bonds and passivation, which lowers the coefficient of friction, cross-hydrogen bonds in the Cr-DLC coating must also be removed [44]. Because of the coating's significant roughness, Cr-GLC has higher initial friction than Cr-DLC, which seems smoother and more coherent. The Cr-DLC showed 30 N after the scratch test, while the Cr-GLC showed 20 N, as shown in Fig.7. The two coatings withstood noticeably higher loads under static or dynamic service conditions as they were extremely tacky and suitable for the substrate. We were able to determine the type of damage to the coating layer system by microscopic examination of scratch marks. Chipping, torsion, spalling, conformal cracking, and tensile cracking are some of the well-defined adhesion failures [30]. Figure 7 shows the scratch track at the beginning of the process. As is typical for bond failure, transverse cracks in the scratch track started as congruent or stress cracks [30]. The Cr-DLC coating degraded with increasing applied load, showing noticeable cracks (Fig.7d), chipping (Fig.7c), and extensive chipping of the coating was observed at the scratch edges. However, the coating of Cr-DLC was also quite complex.

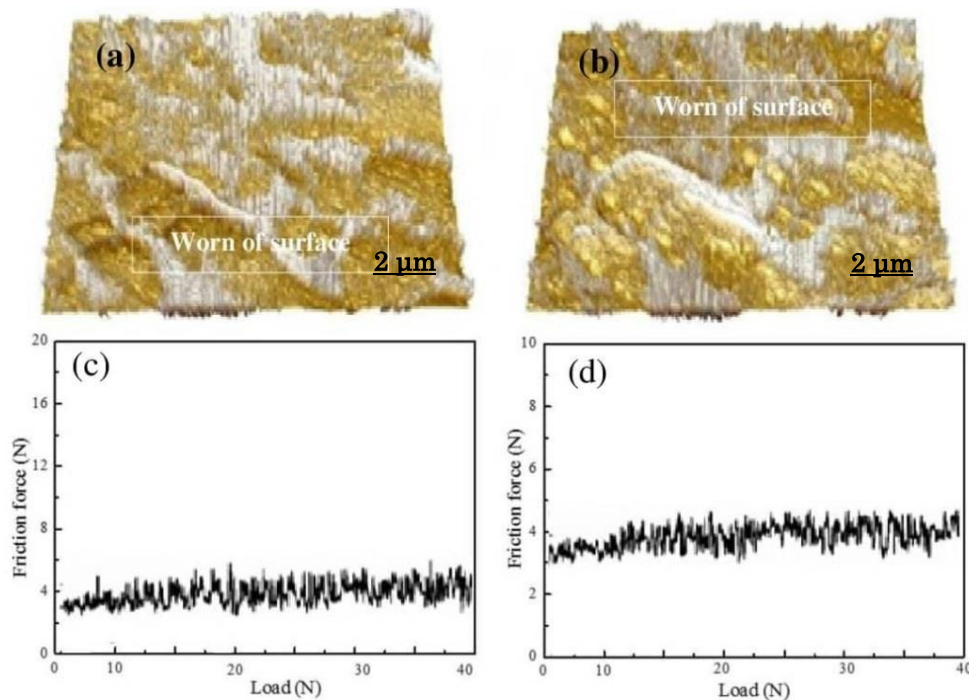


Fig.7. (a) AFM image of the Coating (Cr-GLC) as shown in the AFM image after the scratch test. After the scratch test, the image of the coating (Cr-DLC) is shown in (b). (c) Friction coefficient of the (Cr-DLC) during the test; (d) friction coefficient of (Cr-GLC) during the scratch test.

### 3.8 The coefficient of friction

The coefficient of friction for the lubrication of the two coatings is illustrated in Fig.7. The friction coefficient of lubrication of the layers during the application of both coatings is shown in Fig.7c and d. When there is friction in the (Cr-GLC) system, the reactive film overlaps, traversing a complicated process that results in oscillations during testing. Additionally, at a certain amount of friction, corrosion, and shear stress cause the

curve to change because of the friction surface's increased roughness. In contrast, the dense surface structure of Cr-DLC results in minimal vibration. In addition to the rising concentration of the bonding substance  $sp^3$  C and the coating strength of Cr-DLC [36]. The decreased contact angle causes the film to start forming. With a more consistent coefficient of friction, the Cr-DLC coating offers optimum absorption. Additionally, the low contact angle is the cause of the film that results. Additionally, the boundary lubricant film can be more dependable for coating (Cr-DLC) due to the absence of a C-C structure. The coefficient of friction for coatings of (Cr-DLC) is significantly lower than for coatings of (Cr-GLC) when compared to coating systems. The coating of the layer of Cr-DLC is thicker and more organized as a result of its higher viscosity [15]. The figure displays each coating's friction coefficient under various lubricant conditions. The friction coefficient between the two layers was around 0.10 after drying. However, compared to the dry state, this coefficient of friction is around 40% lower under lubrication. This is because a friction pair can be successfully created by the border lubrication coating and extra adsorption. On both dry and lubricated surfaces, (Cr-DLC) has a lower base coefficient of friction than (Cr-GLC). This is mostly due to the enhanced adhesion between the coating material's particles, which causes the (Cr-DLC) coating to have an inert effect on the surface.

### 3.9. Wear mechanism

To clearly describe the applied surface in a dry and oiled test of two coatings, 3D topography, and SEM morphology were generated as shown in Fig.8. A comparison of the depth of marks generated from the test in both coatings showed that they were less deep when lubricating and deeper under dry test conditions, proving that the use of a solid/liquid combined lubrication system when applying coatings can significantly improve the application resistance in the tribological system [16]. The applied coating of Cr-GLC contains many deep grooves, which show a marked increase in friction and wear rate resulting from the effect of weak bonds of the coating material. The mark on the Cr-DLC coating indicates the applied grooves and residues, as pointed out in Fig.8b. The applied mark of the Cr-GLC coating has a greater depth and width than the coating of Cr-DLC, as clear from in Fig.8c and d, coating. One source for the low hardness of the coating of Cr-GLC is due to complex mineral patterns that can form deep grooves under sliding shear when tested.

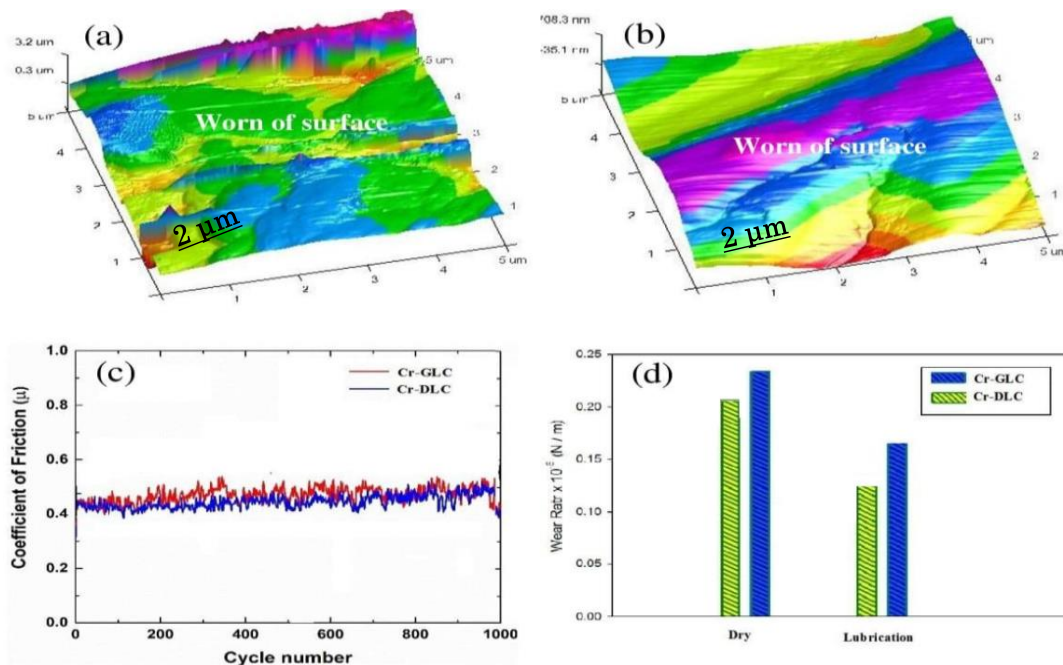


Fig.8. 3D. AFM image of coatings after coating tests (a) (Cr-GLC); and (b) (Cr-DLC): (c) dry friction coefficient; d) dry and lubrication system.

The development of graphitized switching films can also be promoted by additional sp<sup>2</sup>C bonds [46]. The coating shows less wear in the Cr-DLC. Under the test conditions used, the concentration of hydrogen appears to have a significant effect on adhesion, and wear properties but has little to no effect on frictional properties.

On the other hand, the coating of Cr-DLC appears stiffer and has smoother particle cohesion and fewer grooves. Since the applied die has fewer grooves in this coating, it becomes clear that the bonding effect between the two coating particles is a major factor in reducing the wear rate. The SEM morphology revealed numerous particles and grooves on the surface of the two coatings, with larger particles obtained using the coating of Cr-DLC. SEM morphology revealed numerous particles and grooves on the surface of the two coatings in general terms but with deeper grooves obtained when a coating of Cr-DLC was used. In addition, the presence of small layers surrounded by the used particles was shown on the tracks used for each coating.

An EDS assessment was performed in these areas to confirm the excess oxygenated tissue that is trapped in the various tuned areas, as shown in Fig.9a and 9b. The pixel confirms a darker difference in these areas compared to the adjusted one. EDS assessment was performed in the regions of the coatings to confirm the extra tissue in the different regions, as shown in Fig. 9a and 9b. Pixelation confirms a darker difference in these regions of each coating compared to the modified regions. The chemical composition of the scars and particles is shown in Table.2. In addition to C and Cr, the coating of Cr-GLC contains a higher concentration of Si, which is probably due to the fact that the Si particles were concentrated there. Both coatings contain a small amount of O, which may be a result of chemical reactions and friction effects [17].

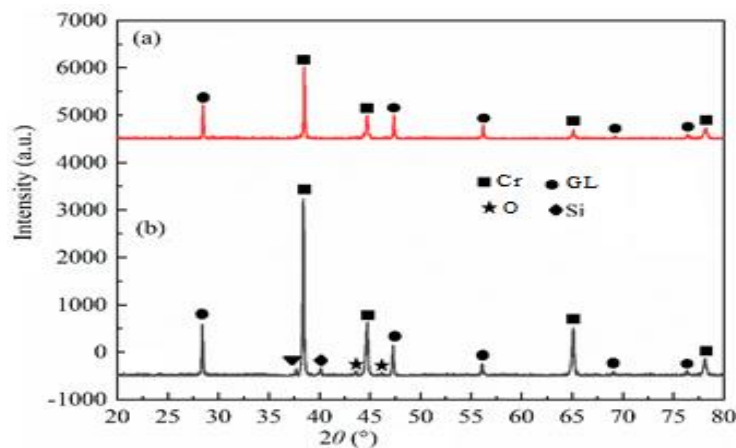


Fig.9. XRD for illustrating the worn surface with small particles scattered, exposed particles in wear track of (a) (Cr-GLC) and (b) (Cr-DLC).

### 3.10. Wear mechanism of coatings tested under conditions of lubrication

Figure 10 displays the cross-sectional profiles and 3D topography of two internally lubricated coatings. The presence of additional wear indicators and significant cracks was confirmed by the coating of Cr-DLC. Increased resistance to plastic deformation can decrease shear, and the presence of extra shear-reducing bonds results in decreased shear prolonging the life of the coatings and reducing wear.

The breathtaking grooves and some of the shallow grooves visible in the applied coating of the Cr-GLC system were validated by the printed mark. A comparison of the depth of marks between the coatings used under all dry and lubricated conditions shows that they are shallower when oiled, which indicates that lubrication can relieve the friction process and reduce adhesion effectively. The lubrication process used had a role in reducing the wear rate of the coatings. corrosion-causing compounds the coating to pass through the rugged columnar structure brought on by significant cracking and frictional shear forces.

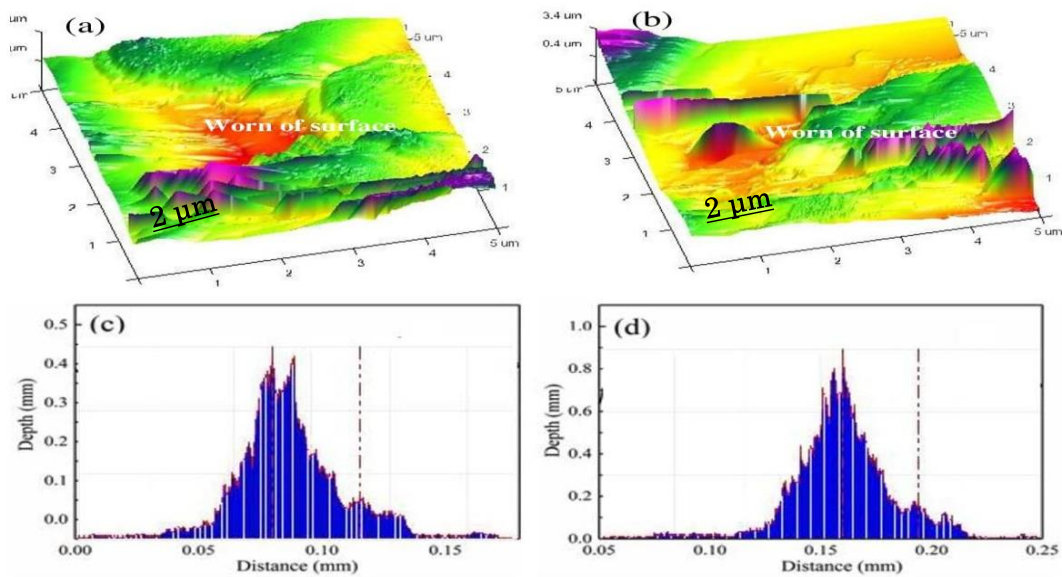


Fig.10. Worn dry surfaces with a wear depth at  $30\text{ N}$  and  $200\text{ rpm}$  in dry sliding, the three-dimensional topography (a) and (c) of the (Cr-GLC), (d) and (b) for (Cr-DLC) coating.

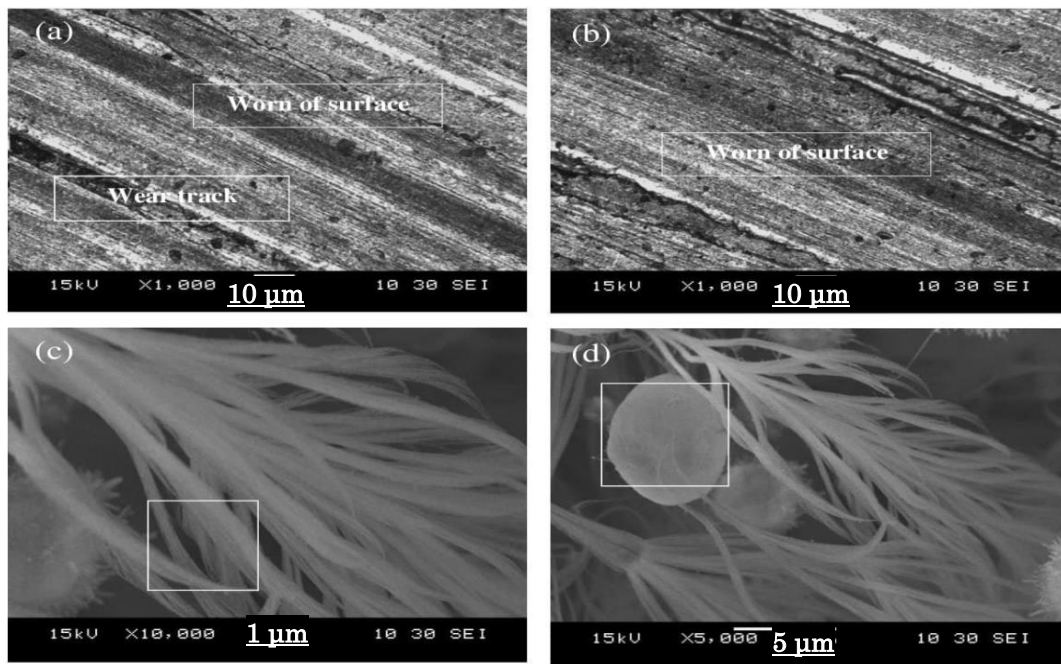


Fig.11. SEM micrograph and X-ray diffractogram of the (a) and (c) wear trace of (Cr-GLC), (b) and (d) wear trace for (Cr-DLC); at  $30\text{ N}$  and  $200\text{ rpm}$  under lubrication.

Figure 11 SEM micrograph and X-ray diffraction pattern of a wear mark (Cr-GLC) and a wear mark (Cr-DLC); at  $30\text{ N}$  and  $200\text{ rpm}$  with lubrication, confirming the schematic description of corrosion applied to (Cr-GLC). The composition is listed in Tab.2, and factors  $B$  and  $E$  verified the excess Fe concentration, which suggests coating degradation. Fe, O and other contents are present, which suggests the occurrence of tribochemical reactions during sliding [18]. Shear resistance increases overall anti-wear performance. Over

time, the shear resistance increases during the testing process due to the accumulation of feathers resulting from the wear process, and the overall performance of wear resistance increases. In contrast, the absorbent film used with lubrication may also interact with the metallic sample and thus may reduce the wear rate.

Analysis of the surface morphology is necessary because good surface morphology improves tribological behavior [20-22]. Figure 12 depicts the coatings' microstructure and surface roughness. The coatings possessed homogeneous particle size distribution and dense morphologies. The coating of Cr-DLC has a smoother surface than the coating of Cr-GLC, which can be seen from their respective surface roughness measurements of  $7.66 \text{ nm}$  and  $2.76 \text{ nm}$ . This conclusion is consistent with the FE-SEM outputs where the Cr-DLC coating is thinner than the Cr-GLC coating. The applied Cr-GLC marks are wider and have more prominent grooves than Cr-DLC, according to a comparison of the two coatings. It is confirmed by the depth of marks that Cr-DLC structures have lubricity. Figure 12 validates the Cr-DLC structures' schematic format. SEM has demonstrated that Cr-DLC is free of significant spots and practically free of significant fissures. The cause is the homogeneity of coating materials and their high resistance to wear and friction [47]. Finally, covalent bonds can be created by ions reacting with the bonds at the base of Cr-GLC coating, reducing wear [49-54]. On another hand, a dense Cr-DLC layer may successfully withstand the wear impacts, offering outstanding tribological performance and pointing to possible directions for future development [54-60].

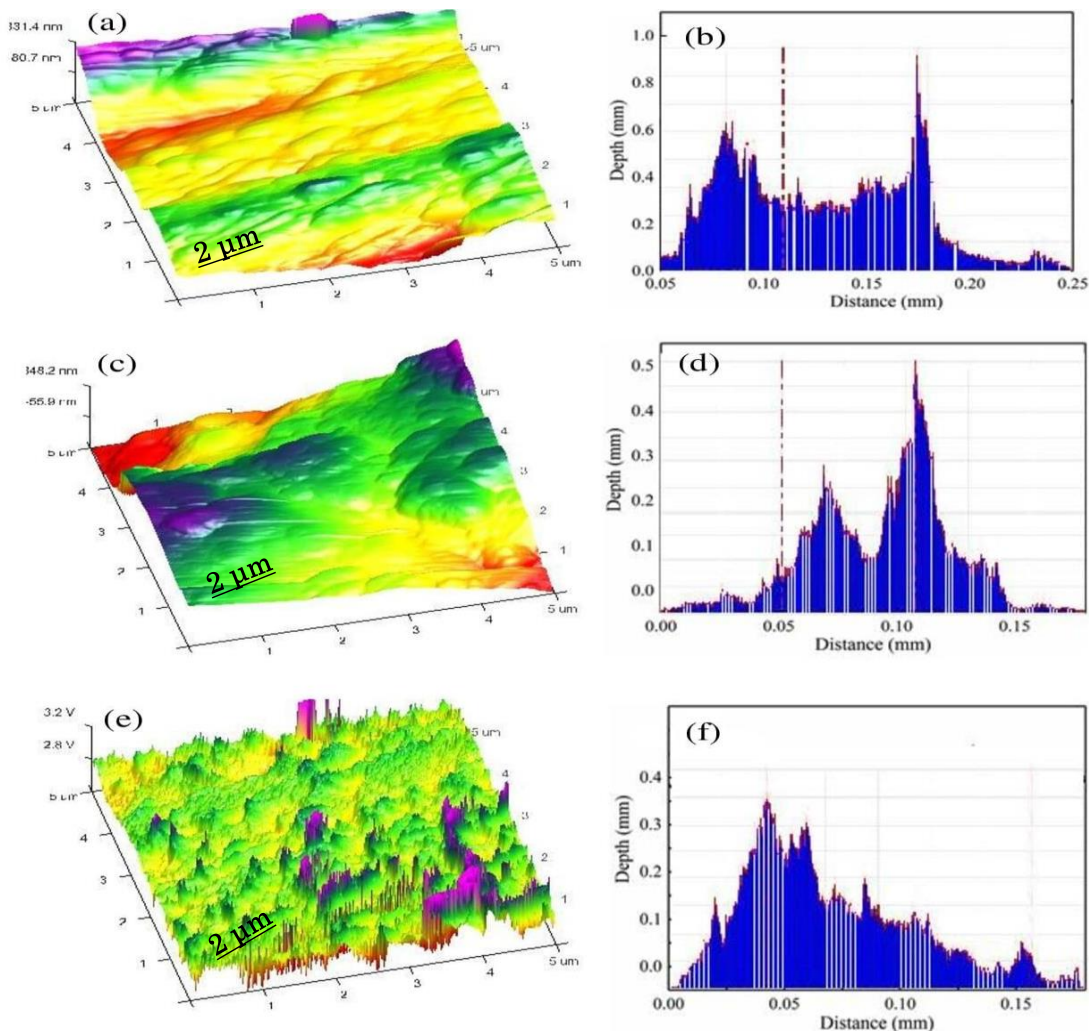


Fig.12. 3D. AFM micrograph of (a) for cross- section with depth (Cr-GLC) and (c) section with depth (Cr-DLC) at  $30N$  and  $200 \text{ rpm}$  under lubrication sliding. 3D topographies; (e) cross-section of (Cr-DLC) at  $10 N$ .

The frictional properties of Cr-DLC, which are ostensibly relatively comparable in composition within the type for both types, are broadly similar, but their wear characteristics can vary greatly. This shows that wear resistance is affected not only by the surface composition. The findings unmistakably show that Cr-DLC coatings are potentially advantageous coatings for lubricated contacts in terms of friction and wear, despite varying wear characteristics. Some Cr-DLC exhibit minimal wear and friction even in the absence of standard lubricant, suggesting that they may be suitable for use in lubricants that do not contain the anti-wear and friction modifiers commonly considered essential in machine component lubricants.

#### 4. Conclusion

In this study, the lubricated Cr-DLC and Cr-GLC coatings' mechanical and tribological properties were examined. The following findings were reached:

1. The coatings of Cr-GLC and Cr-DLC showed high mechanical properties as well as good adhesion to the substrate, and the dense Cr-DLC coating layer assisted in improving these properties.
2. Both coatings have better antifriction and anti-wear benefits. The viscosity and wettability had a direct impact on how well they lubricated as well as the synergistic effect of lubricant quality used.
3. Wear rate had a significant effect on the Cr-GLC system, while it had a limited effect on the Cr-DLC system. In the Cr-DLC lubrication system, abrasive wear exists, while, in Cr-GLC systems, both abrasive wear and corrosive wear are present.

#### Acknowledgement

This work is supported through the University of Samarra. The authors would like to thank the University Sains Malaysia (USM) for all tests which were performed in their laboratories.

#### Nomenclature

Cr-DLC coatings – chromium-doped diamond-like  
 Cr-GLC coatings – chromium-doped graphite carbon

#### References

- [1] Reitschuster S., Maier E., Lohner T., Stahl K., Bobzin K., Kalscheuer C. and Hartl M. (2022): *DLC-coated thermoplastics: tribological analyses under lubricated rolling-sliding conditions.*– Tribology Letters, vol.70, No.4, p.121, <https://link.springer.com/article/10.1007/s11249-022-01664-6>.
- [2] Liu K., Kang J.J., Zhang G.A., Lu Z.B. and Yue W. (2021): *Effect of temperature and mating pair on tribological properties of DLC and GLC coatings under high pressure lubricated by MoDTC and ZDDP.*– Friction, vol.9, pp.1390-1405, <https://link.springer.com/article/10.1007/s40544-020-0420-1>.
- [3] Qiang L., Gao K., Zhang L., Wang J., Zhang B. and Zhang J. (2015): *Further improving the mechanical and tribological properties of low content Ti-doped DLC film by W incorporating.*– Appl. Surf. Sci., vol.353, pp.522-529, <http://dx.doi.org/10.1016/j.apsusc.2015.06.040>.
- [4] Masuko M., Ono T., Aoki S., Suzuki A. and Ito H. (2015): *Friction and wear characteristics of DLC coatings with different hydrogen content lubricated with several Mo-containing compounds and their related compounds.*– Tribol. Int., vol.82, pp.350-357, [https://doi.org/10.1016/S0043-1648\(98\)00314-7](https://doi.org/10.1016/S0043-1648(98)00314-7).
- [5] Hasl C., Illenberger C., Oster P., Tobie T. and Stahl K. (2018): *Potential of oil-lubricated cylindrical plastic gears.*– Journal of Advanced Mechanical Design, Systems, and Manufacturing, vol.12, No.1, p.JAMDSM0016-JAMDSM0016, <https://doi.org/10.1299/jamdsm.2018jamdsm0016>.
- [6] Ziegler A., Maier E., Lohner T. and Stahl K. (2020): *A numerical study on thermal elastohydrodynamic lubrication of coated polymers.*– Tribology Letters, vol.68, No.2, p.71. <https://link.springer.com/article/10.1007/s11249-020-01309>.

- [7] Reitschuster S., Maier E., Lohner T. and Stahl K. (2020): *Friction and temperature behavior of lubricated thermoplastic polymer contacts.*– Lubricants, vol.8, No.6, p.67, <https://doi.org/10.3390/lubricants8060067>.
- [8] Wang L., Guan X., Zhang G. (2013): *Friction and wear behaviors of carbon based multilayer coatings sliding against different rubbers in water environment.*– Tribol. Int., vol.64, pp.69-77, <https://doi.org/10.1016/j.triboint.2013.02.009>.
- [9] Bobzin K., Brögelmann T., Kalscheuer C., Thiex M., Ebner M., Lohner T. and Stahl K. (2018): *A contribution to the thermal effects of DLC coatings on fluid friction in EHL contacts.*– Lubrication Science, vol.30, No.6, pp.285-299. <https://doi.org/10.1002/lis.1421>.
- [10] Li Z., Guan X., Wang Y., Li J., Cheng X., Lu X., Wang L. and Xue Q. (2017): *Comparative study on the load carrying capacities of DLC, GLC and CrN coatings under sliding-friction condition in different environments.*– Surf. Coat Technol., vol.321, pp.350-357, <https://doi.org/10.1016/j.surfcoat.2017.04.065>.
- [11] Aboua K., Umehara N., Kousaka H., Deng X., Tasdemir H., Mabuchi Y., Higuchi T. and Kawaguchi M. (2017): *Effect of carbon diffusion on friction and wear properties of diamond-like carbon in boundary base oil lubrication.*– Tribol. Int., vol.113, pp.389-98, <https://doi.org/10.1016/j.triboint.2016.10.047>.
- [12] Aboua K., Umehara N., Kousaka H., Tokoroyama T., Murashima M., Mabuchi Y., Higuchi T. and Kawaguchi M. (2019): *Effect of carbon diffusion on friction and wear behaviors of diamond-like carbon coating against germanium in boundary base oil lubrication.*– Tribol. Lett., vol.2, pp.65-67, <https://doi.org/10.1007/s11249-019-1179-2>.
- [13] De Barros Bouchet M.I., Martin J.M., Le-Mogne T. and Vacher B. (2005): *Boundary lubrication mechanisms of carbon coatings by MoDTC and ZDDP additives.*– Tribology International, vol.38, No.3, pp.257-264, <https://doi.org/10.1016/j.triboint.2004.08.009>.
- [14] Zhuang W., Fan X., Li W., Li H., Zhang L., Peng J., Cai Z., Mo J., Zhang G. and Zhu M. (2018): *Comparing space adaptability of diamond-like carbon and molybdenum disulfide films toward synergistic lubrication.*– Carbon vol.134, pp.163-173, <https://doi.org/10.1016/j.carbon.2018.03.059>.
- [15] Maier E., Ziegler A., Lohner T. and Stahl K. (2017): *Characterization of TEHL contacts of thermoplastic gears.*– Forschung im Ingenieurwesen, vol.81, No.2-3, pp.317-324, <https://link.springer.com/article/10.1007/s10010-017-0230-4>.
- [16] Feng X. and Xia Y. (2012): *Tribological properties of Ti-doped DLC coatings under ionic liquids lubricated conditions.*– Appl. Surf. Sci., vol.258, pp.2433-2438, <https://doi.org/10.1016/j.apsusc.2011.10.066>.
- [17] Rothhammer B., Marian M., Neusser K., Bartz M., Böhm T., Krauß S. and Wartzack S. (2021): *Amorphous carbon coatings for total knee replacements. Part II: Tribological behavior.*– Polymers, vol.13, No.11, p.1880, <https://doi.org/10.3390/polym13111880>.
- [18] Rothhammer B., Neusser K., Marian M., Bartz M., Krauß S., Böhm T. and Wartzack S. (2021): *Amorphous carbon coatings for total knee replacements. Part I: Deposition, cytocompatibility, chemical and mechanical properties.* Polymers, vol.13, No.12, p.1952, <https://doi.org/10.3390/polym13121952>.
- [19] Sui X., Liu J., Zhang S., Yang J. and Hao J. (2018): *Microstructure, mechanical and tribological characterization of CrN/DLC/Cr-DLC multilayer coating with improved adhesive wear resistance.*– Appl. Surf. Sci., vol.439, pp.24-32, <https://doi.org/10.1016/j.apsusc.2017.12.266>.
- [20] Bobzin K., Kalscheuer C., Thiex M., Sperka P., Hartl M., Reitschuster S. and Stahl K. (2023): *DLC-Coated Thermoplastics: Tribological Analyses Under Dry and Lubricated Sliding Conditions.* Tribology Letters, vol.71, No.1, p.2, <https://link.springer.com/article/10.1007/s11249-022-01663-7>.
- [21] Jo Y., Zhang T., Son M. and Kim K. (2018): *Synthesis and electrochemical properties of Ti-doped DLC films by a hybrid PVD/PECVD process.*– Appl. Surf. Sci., vol.433, pp.1184-91, <https://doi.org/10.1016/j.apsusc.2017.10.151>.
- [22] Khalaj Z., Ghoranneviss M., Vaghri E., Saghaleini A. and Diudea M.V. (2012): *Deposition of DLC film on stainless steel substrates coated by nickel using PECVD method.*– Acta Chim. Slov. vol.59, p.338. <https://pubmed.ncbi.nlm.nih.gov/24061250/>.
- [23] Ebrahimi M., Mahboubi F. and Naimi-Jamal M. (2015): *Wear behavior of DLC film on plasma nitrocarburized AISI 4140 steel by pulsed DC PACVD: effect of nitrocarburizing temperature.*– Diam. Relat. Mater., vol.52, pp.32-37, <https://doi.org/10.1016/j.diamond.2014.12.004>.
- [24] Dong D., Jiang B., Li H., Du Y. and Yang C. (2018): *Effect of graphite target power density on tribological properties of graphite-like carbon films.*– Appl. Surf. Sci., vol.439, pp.900-909. <https://doi.org/10.1016/j.apsusc.2018.01.113>.
- [25] Yilmaz M., Lohner T., Michaelis K. and Stahl K. (2019): *Minimizing gear friction with water-containing gear fluids.*– Forschung im Ingenieurwesen, vol.83, No.3, pp.327-337, <https://doi.org/10.1007/s10010-019-00373-2>.
- [26] Al-Samarai R.A., Haftirman K.R.A. and Al-Douri Y. (2012): *The influence of roughness on the wear and friction coefficient under dry and lubricated sliding.*– Int. J. Sci. Eng. Res., vol.3, No.4, pp.1-6.

- [27] Ziegltrum A., Maier E., Lohner T. and Stahl K. (2020): *A numerical study on thermal elastohydrodynamic lubrication of coated polymers.*– Tribology Letters, vol.68, No.2, p.71, <https://link.springer.com/article/10.1007/s11249-020-01309-6>.
- [28] Wu D., Ren S., Pu J., Lu Z., Zhang G. and Wang L.A. (2018): *Comparative study of tribological characteristics of hydrogenated DLC film sliding against ceramic mating materials for helium applications.*– Appl. Surf. Sci., vol.441, pp.884-894, <https://doi.org/10.1016/j.apsusc.2018.01.206>.
- [29] Chen L., Liu Z. and Shen Q. (2018): *Enhancing tribological performance by anodizing micro-textured surfaces with nano-MoS<sub>2</sub> coatings prepared on aluminum-silicon alloys.*– Tribol. Int., vol.122, pp.84-95, <https://doi.org/10.1016/j.triboint.2018.02.039>.
- [30] Sun J., Fu Z., Zhang W., Wang C., Yue W., Lin S. and Dai M. (2013): *Friction and wear of Cr-doped DLC films under different lubrication conditions.*– Vacuum, vol.94, pp.1-5, <https://doi.org/10.1016/j.vacuum.2013.01.010>.
- [31] Tokoroyama T., Hattori T., Umehara N., Kousaka H., Manabe K., Kishi M. and Fuwa Y. (2016): *Ultra-low friction properties of carbon nitride tantalum coatings in the atmosphere.*– Tribol. Int., vol.103, pp.388-393, <https://doi.org/10.1016/j.triboint.2016.07.015>.
- [32] Al-Douri Y., Al-Samarai R.A., Abdulateef S.A., Odeh A.A., Badi N. and Voon C.H. (2019): *Nanosecond pulsed laser ablation to synthesize GaO colloidal nanoparticles: Optical and structural properties.*– Optik, vol.178, pp.337-342, <https://doi.org/10.1016/j.ijleo.2018.09.158>.
- [33] Qi J., Wang L., Yan F. and Xue Q. (2013): *The tribological performance of DLC-based coating under the solid-liquid lubrication system with sand-dust particles.*– Wear, vol. 297, pp.972-985, <https://doi.org/10.1016/j.wear.2012.11.015>.
- [34] Duminica F., Belchi R., Libralesso L. and Mercier D. (2018): *Investigation of Cr(N)/DLC multilayer coatings elaborated by PVD for high wear resistance and low friction applications.*– Surf. Coat. Technol., vol.33, pp.396-403, <https://doi.org/10.1016/j.surfcoat.2018.01.052>.
- [35] Cao Z., Xia Y., Liu L. and Feng X. (2019): *Study on the conductive and tribological properties of copper sliding electrical contacts lubricated by ionic liquids.*– Tribol. Int., vol.130, pp.27-35, <https://doi.org/10.1016/j.triboint.2018.08.033>.
- [36] Zhang S. and Zhang X. (2012): *Toughness evaluation of hard coatings and thin films.*– Thin Solid Films, vol.520, pp.2375-2389, <https://doi.org/10.1016/j.tsf.2011.09.036>.
- [37] Bai W., Li L., Xie Y., Liu D., Wang X., Jin G. and Tu J. (2016): *Corrosion and tribocorrosion performance of M (M = Ta, Ti) doped amorphous carbon multilayers in Hank's solution.*– Surf. Coat Technol., vol.305, pp.11-22, <https://doi.org/10.1016/j.surfcoat.2016.07.078>.
- [38] He D., Shang L., Lu Z., Zhang G., Wang L. and Xue Q. (2017): *Tailoring the mechanical and tribological properties of B<sub>4</sub>C/a-C coatings by controlling the boron carbide content.*– Surf. Coat Technol. vol.329, pp.11-18. <https://doi.org/10.1016/j.surfcoat.2017.09.017>.
- [39] Reitschuster S., Maier E., T. Lohner T., Stahl K., Bobzin K., Kalscheuer C., Thiex M., Sperka P. and Hartl M. (2022): *DLC-coated thermoplastics: tribological analyses under lubricated rolling-sliding conditions.*– Tribology Letters, vol.70, Article No.121, pp.1-16, <https://doi.org/10.1007/s11249-022-01664-6>
- [40] Neuville S. (2011): *Quantum electronic mechanisms of atomic rearrangements during growth of hard carbon films.*– Surf. Coat Technol., vol.206, pp.703-726, <https://doi.org/10.1016/j.surfcoat.2011.07.055>.
- [41] Ye Y., Wang Y., Chen H., Li J., Yao Y. and Wang C. (2015): *Doping carbon to improve the tribological performance of CrN coatings in seawater.*– Tribol. Int., vol.90, pp.362-371, <https://doi.org/10.1016/j.triboint.2015.04.008>.
- [42] Hua C., Guo J., Liu J., Yan X., Zhao Y., Chen L., Wei J., Hei L. and Li C. (2016): *Influence of diamond surface chemical states on the adhesion strength between Y<sub>2</sub>O<sub>3</sub> film and diamond substrate.*– Mater. Des., vol.105, pp.81-88, <https://doi.org/10.1016/j.matdes.2016.05.026>.
- [43] Zhu S. and Huang P. (2017): *Influence mechanism of morphological parameters on tribological behaviors based on bearing ratio curve.*– Tribol. Int., vol.109, pp.10-18, <https://doi.org/10.1016/j.triboint.2016.12.014>.
- [44] Erdemir A. (2001): *The role of hydrogen in tribological properties of diamond-like carbon films.*– Surf. Coat Technol., vol.146, pp.292-297, [https://doi.org/10.1016/S0257-8972\(01\)01417-7](https://doi.org/10.1016/S0257-8972(01)01417-7).
- [45] Al-Samarai R.A. and Al-Douri Y. (2018): *Lubricated conditions imposed on coating multi-layer on wear resistance under Cr<sub>2</sub>O<sub>3</sub> effect.*– Materials Research, vol.21, No.4, <http://dx.doi.org/10.1590/1980-5373-mr-2017-0938>.
- [46] Gilewicz A., Warcholinski B. (2014): *Tribological properties of CrCN/CrN multilayer coatings.*– Tribol. Int., vol.80, pp.34-40, <https://doi.org/10.1016/j.triboint.2014.06.012>.
- [47] Han Y., Qiao D., Zhang S. and Feng D. (2017): *Influence of phosphate and phosphonate ionic liquid structures on lubrication for different alloys (Mg, Al, Cu).*– Tribol. Int., vol.114, pp.469-477, <https://doi.org/10.1016/j.triboint.2017.05.019>.

- [48] Liu X., Pu J., Wang L. and Xue Q. (2013): *Novel DLC/ionic liquid/graphene nanocomposite coatings towards high-vacuum related space applications.*– J. Mater. Chem., vol.1, pp.3797-3809, <https://doi.org/10.1039/C3TA00764B>.
- [49] Paul D. (2023): *Fretting wear behavior of aluminum coatings.*– Experimental and Theoretical NANOTECHNOLOGY, vol.7, pp.257-267, <https://doi.org/10.56053/7.2.257>.
- [50] Fuji J., Shuji T., Jumbo F., Saraki G. and Tanemura M. (2023): *Optical analysis of multi-crystalline Si surface.*– Experimental and Theoretical NANOTECHNOLOGY, vol.7, pp.273-282, <https://doi.org/10.56053/7.2.273>.
- [51] Pasal M.C. and Aras C.M. (2023): *Investigation of semi-metallic properties of GdS band TbSb compounds.*– Experimental and Theoretical NANOTECHNOLOGY, vol.7, pp.371-380, <https://doi.org/10.56053/7.2.371>.
- [52] Jabbar O. and Reshak A.H. (2023): *Structural, electronic, and optoelectronic properties of XYZZ (X=Zn,Cd; Y=Si,Sn;Z=pnicogens) chalcopyrite compounds: first-principles calculations.*– Experimental and Theoretical NANOTECHNOLOGY, vol.7, pp.97-110, <https://doi.org/10.56053/7.1.97>.
- [53] Li L. and Naher S. (2023): *Half-metallic behavior Co<sub>2</sub>YAl (Y= Mo,Tc) compounds.*– Experimental and Theoretical NANOTECHNOLOGY, vol.7, pp.127-138, <https://doi.org/10.56053/7.1.172>.
- [54] Christ J., Filips M., Artois S., Nowak R., Reed M. and Knoll W. (2023): *Sliding wear of rubber/layered silicate nanocomposites.*– Experimental and Theoretical NANOTECHNOLOGY, vol.7, pp.159-170, <https://doi.org/10.56053/7.1.195>.
- [55] Al-Jassim M., Grüner G. and Guo J. (2022): *GaN on Si (111) nanostructure for solar cells application.*– Experimental and Theoretical NANOTECHNOLOGY, vol.6, pp.447-452, <https://doi.org/10.56053/6.4.447>.
- [56] Felser C., Kaskel S. and Rubio A. (2022): *Surface ion with Mo, Ti and Al for steel studies.*– Experimental and Theoretical NANOTECHNOLOGY, vol.6, pp.477-484, <https://doi.org/10.56053/6.4.477>.
- [57] Sharma S. (2022): *In-doped aluminum antimonide alloy for optoelectronic applications.*– Experimental and Theoretical NANOTECHNOLOGY, vol.6, pp.295-316, <https://doi.org/10.56053/6.3.592>.
- [58] Alex S. (2022): *Micro-size aluminum for environmental detonation.*– Experimental and Theoretical NANOTECHNOLOGY, vol.6, pp.333-345, <https://doi.org/10.56053/6.3.333>.
- [59] Ismail O. (2022): *Analysis of localized corrosion on stainless steel.*– Experimental and Theoretical NANOTECHNOLOGY, vol.6, pp.209-222, <https://doi.org/10.56053/6.2.209>.
- [60] Sealen M. and Engstrom O. (2022): *Morphological studies of Si nanowires effect on the photovoltaics.*– Experimental and Theoretical NANOTECHNOLOGY, vol.6, pp.53-60, <https://doi.org/10.56053/6.1.53>.

Received: January 4, 2023

Revised: September 22, 2023